RETRIEVAL OF PRECIPITATION AND COLUMNAR WATER VAPOUR CONTENT FROM AMSU-A/B

R.Bennartz [1] , A.Thoss, and J.Fischer
Institute for Space Sciences
Free University of Berlin, Germany

1 INTRODUCTION

Besides it's main dedication to provide water vapour and temperature sounding information the Advanced Microwave Sounding Unit (AMSU) onboard NOAA-K allows to derive hydro-meteorological parameters, such as columnar water vapour content, cloud liquid water, and precipitation. These parameters are necessary for monitoring the global energy and water cycle and for other climatological applications. In this study algorithms to derive surface rain rates (RR) and water vapour path (WVP) over open water surfaces are introduced. Both algorithms are based on inversion of radiative transfer simulations. While for WVP a linear regression algorithm is employed, for RR linear regression is compared to the results of a neural network.

2 METHOD

2.1 Radiative Transfer Simulations

All radiative transfer calculations were performed using a polarized eddington model described in Bauer and Bennartz (1997). Gaseous absorption was calculated using the algorithm of Liebe (1985). The emissivity of the ocean surface was parameterized according to Schlüssel and Luthardt (1991). Different cloud types were adapted to the model with liquid water contents and droplet size distributions according to Silverman and Sprangue (1970). All ice particles were assumed to be spherical and to have the same distribution as liquid water droplets. Both phases were allowed to occur at the same level, the relation between ice and liquid water was determined according to Wu and Weimann (1984). The droplet size distribution and intensity of rain was parameterized using the Marshall-Palmer approach. For size parameters greater than 0.1 Mie-scattering was applied.

The model was applied to 1477 globally distributed radiosoundings taken in the period from August 1987 to August 1988. First, for each radiosounding a cloud-free simulation was performed. Second, an additional cloudy simulation was performed, if the relative humidity at one or more levels exceeded 95 % (valid for 245 radiosoundings). To account to first order for beam-filling each cloudy simulation was mixed to a randomly varied extend with the corresponding cloud-free simulation leading to combinations of simulations describing partially cloudy situations. Three dimensional radiative transfer

[1]Corresponding author address: Ralf Bennartz, Institute for Space Sciences, Free University of Berlin, Fabeckstr.69, 14195 Berlin, e-mail: bennartz@zedat.fu-berlin.de

effects are still not included.

The same method was applied to simulations including precipitation (and clouds). First simulations were performed with precipitation (on the 245 radiosoundings mentioned above). These were randomly mixed with cloudy and cloud-free simulations.

Simulations were performed for the channels listed in Table 1 for the zenith angles $\theta = 0, 10, 20, 30, 40, 50, 60 deg$. A randomly distributed gaussian noise was added to each simulation. The rotation of the polarization plane of the AMSU measurements was taken account for, cross-polarization coupling was neglected.

3 RETRIEVAL OF WATER VAPOUR CONTENT

To allow for the derivation of WVP even in cloudy situations, the use of low frequency AMSU-A channels is desirable, since at low frequencies the transmissivity of non-precipitating clouds is high. However, emission of cloud liquid water considerably affects the measured brightness temperatures. Experiences with the Special Sensor Microwave/Imager SSM/I (Schlüssel and Emery, 1990) suggest the use of a two frequency algorithm to derive WVP and simultaneously correct for liquid water emission. The following models for the derivation of WVP are examined:

$$q = a_0 + a_1 * log(310.0 - T_{B23}) + a_2 * log(310.0 - T_{B31}), \quad (1)$$

$$q = a_0 + a_1 * log(310.0 - T_{B23}) + a_2 * log(310.0 - T_{B31}) + a_3 * log(310.0 - T_{B23})^2, \quad (2)$$

where q is the WVP and T_{B23} and T_{B31} are the measured brightness temperatures at 23.8 GHz and at 31.4 GHz, respectively. Since the zenith angle and the polarization state of the measurements varies with the AMSU's scan position (see Table 1), the regression coefficients were derived for all zenith angle considered in the radiative transfer simulations. The regression coefficients a_i were obtained from the cloudy dataset by excluding clouds with liquid water path higher than $300 g/m^2$. This threshold has been chosen since non-precipitating clouds with liquid water path higher than $300 g/m^2$ are considered to be unlikely (Grody, 1993).

For model 1 the dependency of the regression constants and of the rms-error of the regression on zenith angle is shown in Figure 1. The variation of the regression coefficients a_i with zenith angle is small, as is the variation of the rms-error. A moderate increase of rms-error associated with decreasing a_i's towards high zenith angles can be observed, reflecting the increasing optical thickness of the atmosphere.

Figure 2 shows the rms-error and the bias of the regression model 1 as functions of the WVP. Even though the rms-error does not exceed $2.2 kg/m^2$ and the overall rms-error is small ($1.44 kg/m^2$), a significant dependency of bias on WVP is found. While for values less than about $20 kg/m^2$ WVP is underestimated, a systematic overestimation of WVP occurs for values higher than $25 kg/m^2$. A similar but weaker trend has been observed for WVP retrieval algorithms for the SSM/I (Schlüssel

and Emery, 1990). The introduction of a quadratic term in model 2 corrects for this behaviour. As shown in Figures 3 and 4, the variation of regression coefficients with zenith angle increases. Especially the regression constant a_0 and the quadratic term represented by a_3 show significant dependencies on zenith angle. The signal dependent bias decreases. Only water vapour contents below $10kg/m^2$ appear to be systematically underestimated. Between $10kg/m^2$ and $60kg/m^2$ no systematic trends occur.

4 RETRIEVAL OF PRECIPITATION

For the retrieval of precipitation two different methods were compared. First, a multispectral regression was established. Second, a backpropagation neural network was trained based on the same input dataset as used for the regression. The regression model is given by

$$RR = a_0 + a_1 * log(310.0 - T_{B23}) + a_2 * log(310.0 - T_{B31}) + a_3 * log(310.0 - T_{B52.8}) + a_4 * log(310.0 - T_B 150) \quad (3)$$

Figure 5 shows the dependency of the regression constants and the rms-error of the regression model on zenith angle. The comparably small rms-error is dominated by small rain rates occuring more frequently in the dataset than higher rain rates. This has been taken account for in the regression by weighting the relative contribution of each simulation with the rain rate dependent inverse density of simulations. Hence, the impact of densely represented areas on the regression coefficients is reduced, while the impact of sparsely represented areas is enhanced. A more meaningful representation of the errors associated with the regression model is given Figure 6. A significant signal dependent trend in bias and rmse is observed for the regression model. The introduction of higher order terms as successfully demonstrated for WVP did not yield better results for this case.

The neural network consists of four input neurons, 10 hidden layer neurons and one output neuron. Each neuron of a given layer is connected to every neuron of the previous layer. The input neurons are fed with the brightness temperatures of the same channels as used in the regression model. Due to constraints of the neural network's architecture the input channels had to be linearly transformed to a range between $]0, 1[$. The output neuron represents the surface rain rate, again calibrated to values between $]0, 1[$. Since the network's number of free parameters is much higher than the regression's free parameters, the entire simulation dataset had to be split in two seperate datasets dedicated for either training or testing the network.

Figure 7 shows the results of the network for the test dataset. Up to 7 mm/h rain rate no trend in bias can be observed. For rain rates higher than 7 mm/h the network underestimates rain rate systematically. Obviously, the network better represents the relation between rain rate and simulated brightness temperatures than the regression model. The underestimation of high rain rates may have physical reasons. The channels used for the retrieval are mainly located in the emission region below 50-60 GHz. In this frequency domain emission of liquid cloud and precipitation droplets leads to an increase of the simulated brightness temperatures compared to the cold brightness temperatures

observed for cloud- and precipitation-free atmospheres over ocean. Since this signal is directly related to liquid precipitation, it is the most directly coupled with surface rain rate. The simulations show saturation of this emission signal at about 7 mm/h for 31.4 GHz. This indicates that the bias of the network above 7mm/h is physically determined. Although the impact of the spatial resolution of the AMSU-A on brightness temperatures observed is not investigated in this study, Bauer and Bennartz (1997) addressed this issue for a different sensor, but with comparable spatial resolution (for the Tropical Rainfall Measuring Mission's (TRMM) TRMM Microwave Imager (TMI)). Even for the heavily precipitating large convective system examined in this investigation area averaged precipitation rates above 8-10mm/h did not occur. Further problems using the emission signal at low frequencies arise from emission of cloud liquid water deteriorating the emission signal of precipitation. The relative importance of cloud liquid water emission increases with increasing frequency. While frequencies lower than 20 GHz are only weakly affected by cloud liquid water, frequencies above 30 GHz are strongly influenced.

Besides the emission signal at low frequencies, scattering of precipitation-sized ice particles at higher frequencies may allow to identify and quantify precipitation. However, the relation between large ice particles at cloud top and surface precipitation rate is highly non-linear. The use of the scattering signal at window frequencies above 50 GHz in inverse modelling techniques requires more complete cloud and precipitation models, describing the relation between the amount of high level precipitation-sized ice particles and surface rain rate. Simple cloud models as used in this study fail to render these complex microphysical relations.Improvements may either be achieved by using radar measurements describing the vertical and horizontal distribution of precipitation particles within clouds (Bauer et al., 1996; Bauer and Bennartz, 1997) or by employing coupled hydrodynamical and microphysical models describing cloud dynamics.

An empirical approach to derive precipitation information from the scatttering signal would be to adjust the relation between the observed brightness temperatures and rain rates by means of colocated radar or rain gauge measurements. Simmer (1996) emphasizes the need for calibration of algorithms based on the scattering signal.

5 SUMMARY AND CONCLUSIONS

Retrieval algorithms for columnar water vapour content and precipitation were established. These algorithms were developed for channel combinations available at AMSU-A/B. WVP can be derived from low frequency AMSU-A measurements. This allows for the derivation of WVP even in overcast situations with high liquid water path ($LWP < 300 kg/m^2$). The standard error of the retrieval is in the order of $1.5 kg/m^2$.

Retrieval of precipitation is investigated comparing a linear regression model with a neural network. While the regression method leads to significant underestimation of high rain rates, the neural network results are in better agreement with the simulations. However, retrieval of rain rates using AMSU suffers from the lack of low frequency channels (below 20 GHz). The lowest available frequencies at

23.8 GHz and 31.4 GHz are strongly affected by columnar water vapour content and cloud liquid water, respectively. Further efforts will concentrate on a consistent physical approach to derive precipitation information including sensor geometry as well as cloud microphysical and dynamical effects.

6 ACKNOWLEDGMENTS

The authors would like to thank Dr. P. Bauer for providing the radiative transfer model.

7 LITERATURE

Bauer, P., L. Schanz, R. Bennartz, and P. Schluessel, 1997: Outlook for combined TMI-VIRS algorithms for TRMM: Lessons from the PIP and AIP projects. J. Atmos. Sciences in press.

Bauer, P. and R. Bennartz, 1997: TMI Imaging capabilities for the observation of rainclouds. Submitted to Radio Science.

Grody, N.C. 1993: Remote Sensing of the Atmosphere from Satellites using microwave radiometry. In: Atmospheric Remote Sensing by Microwave Radiometry. Ed. M.A. Janssen, Wiley Interscience Publications, New York.

Liebe, H.J. 1985: An updated model for millimeter wave propagation in moist air. Radio Science, 20, No.5, 1069-1089.

Saunders, R.W., S.J. English, and D.C. Jones, 1994: AMSU-B a new tool for atmospheric research. SPIE, Vol. 2313, 98-107.

Schluessel, P. and W. J. Emery, 1990: Atmospheric water vapour over oceans from SSM/I measurements. Int.J. Rem.Sens.11, 753-766.

Schluessel, P. and H.Luthardt, 1991: Surface wind speeds over ocean from Special Sensor Microwave/Imager observations. J.Geophys.Res.96, C3, 4845-4853.

Simmer, C. 1996: Retrieval of precipitation from satellites. In: Radiation and Water in the Climate System. Ed.: E. Raschke, Springer-Verlag, Berlin, 1996.

Silverman, B.A. and E.D. Sprangue, 1970: Airborne measurements of in-cloud visibility. Nat.Conf. on Weather Modification of the AMS, April 6-9, Santa Barbara CA.

Wu, R. and J.A. Weinman, 1984: Microwave radiances from precipitating clouds containing aspherical ice, combined phase and liquid hydrometeors. J.Geophys.Res., 89, D5, 7170-7178.

Frequency $[GHz]$	Bandwidth $[GHz]$	NEΔT $[K]$	Polarization $[deg]$
23.8	0	0.22	90-Θ
31.4	0	0.21	90-Θ
50.3	0	0.28	90-Θ
52.8	0	0.20	90-Θ
180.3/3.0	1.0	0.70	90-Θ
180.3/1.0	0.5	1.06	90-Θ
183.3/7.0	2.0	0.60	90-Θ
90.0/0.9	1.0	0.37	90-Θ
150.0/0.9	1.0	0.84	90-Θ

Table 1 : AMSU-A/B channels for which radiative transfer simulations were carried out. NEΔT and Polarization values are taken from Saunders et al. (1994) .

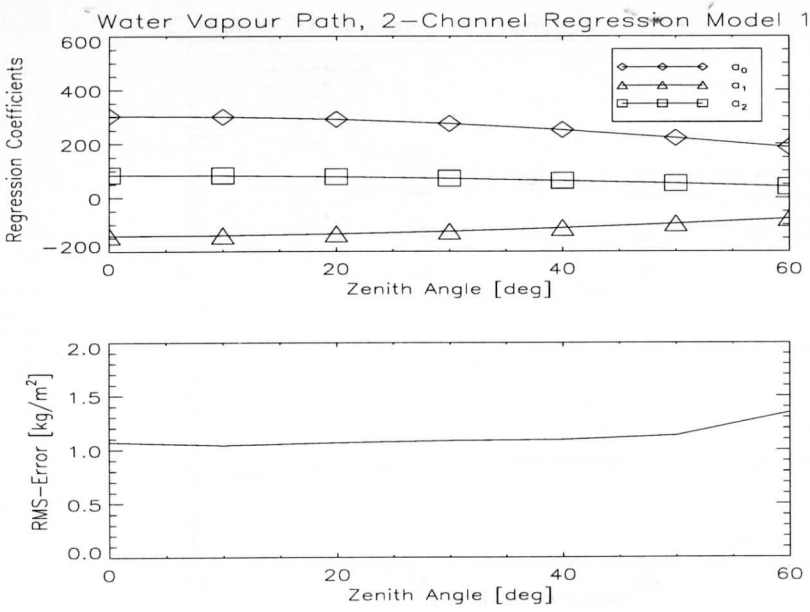

Figure 1 : Dependency of water vapour retrieval regression coefficients (upper panel) and rms-error of regression on zenith angle for regression model 1 (upper panel).

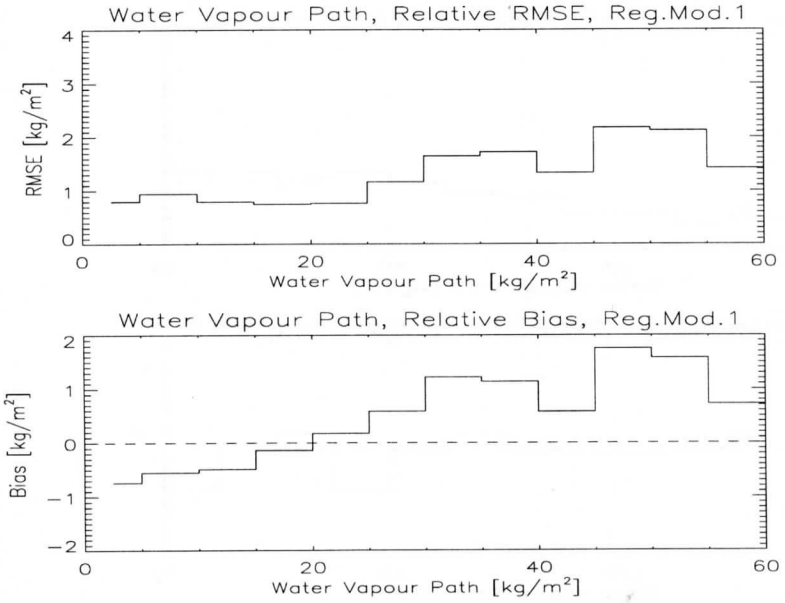

Figure 2 : Rms-error and bias of water vapour regression model 1 with respect to the simulation's water vapour content.

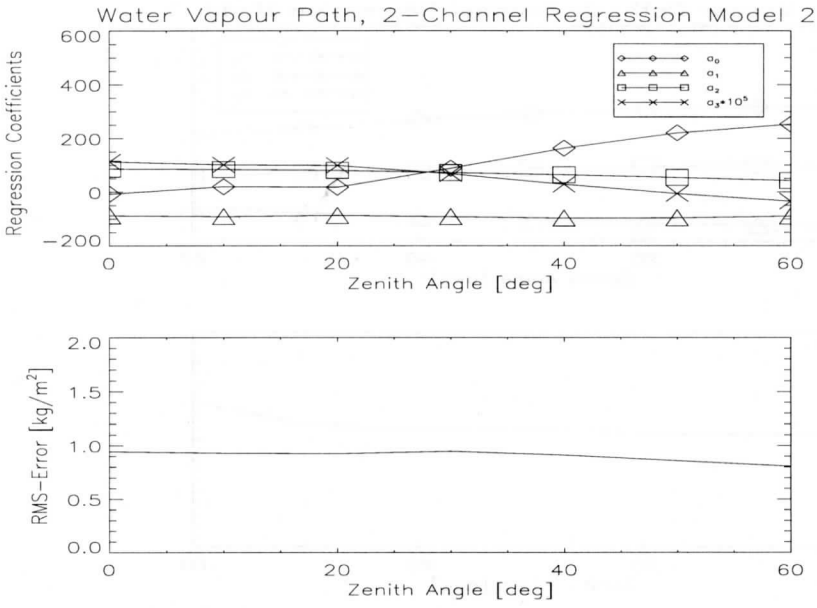

Figure 3 : Dependency of water vapour retrieval regression coefficients (upper panel) and rms-error of regression on zenith angle for regression model 2 (upper panel).

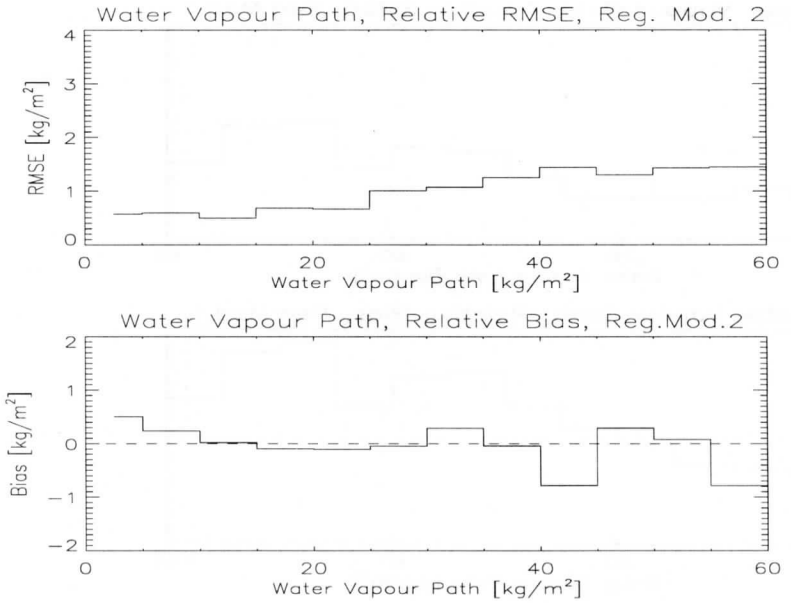

Figure 4 : Rms-error and bias of water vapour regression model 2 with respect to the simulation's water vapour content.

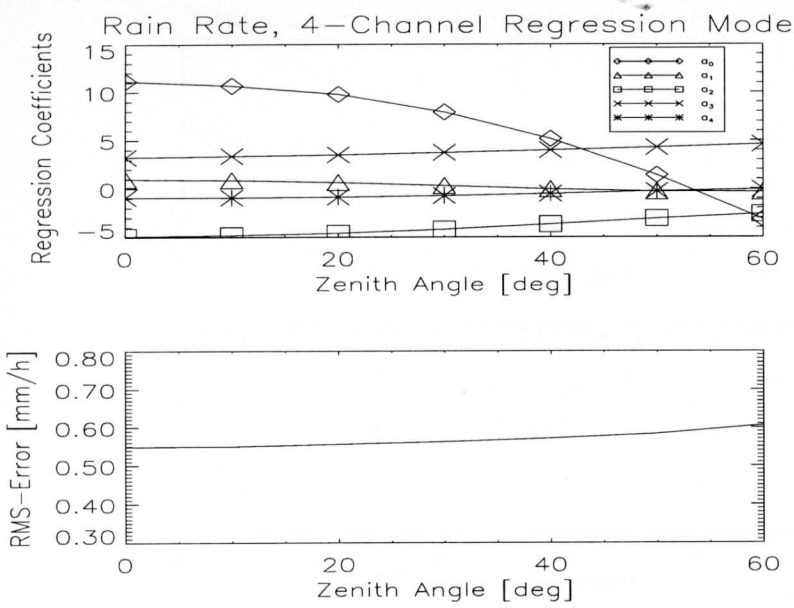

Figure 5 : Dependency of the surface rain rate retrieval regression coefficients (upper panel) and rms-error of regression on zenith angle for regression model 2 (upper panel).

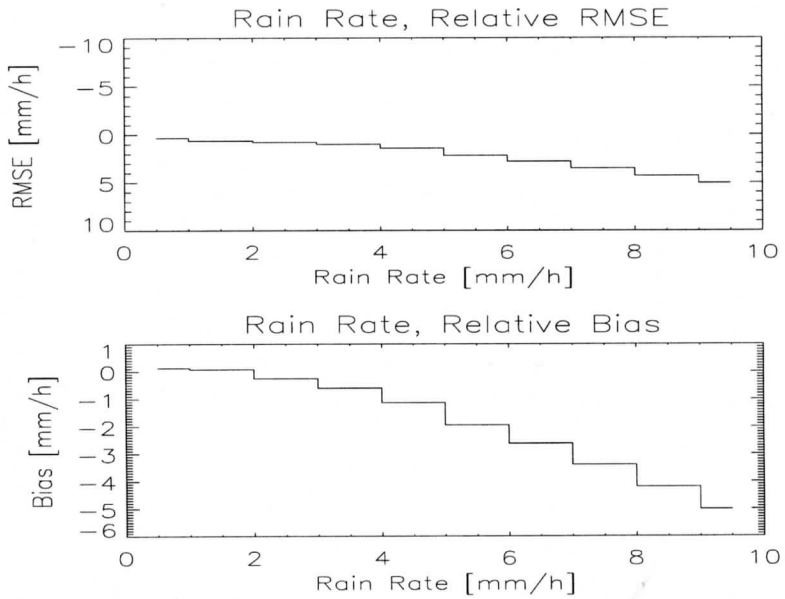

Figure 6 : Rms-error and bias of the surface rain rate regression model with respect to the simulation's rain rate.

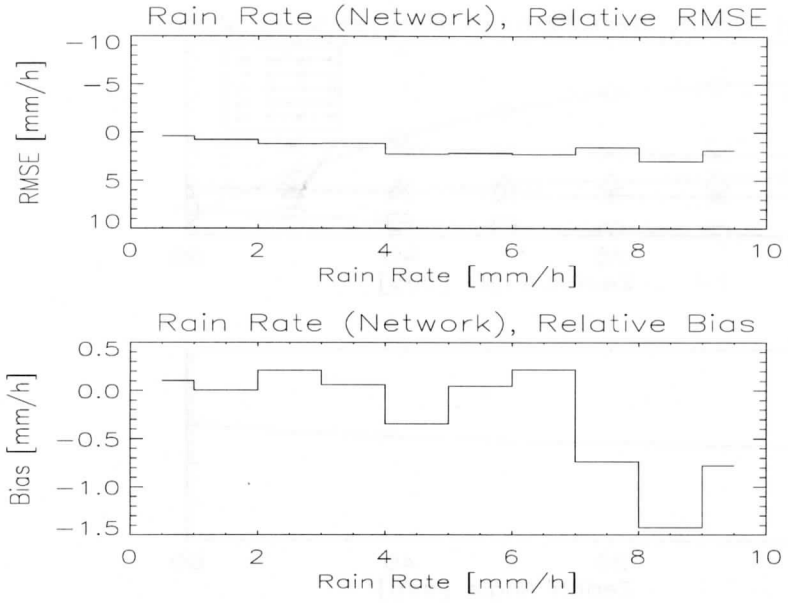

Figure 7 : Rms-error and bias of the neural network's surface rain rate estimate with respect to the simulation's rain rate.

TECHNICAL PROCEEDINGS OF

THE NINTH INTERNATIONAL TOVS STUDY CONFERENCE

Igls, Austria

20-26 February 1997

Edited by

J R Eyre

Meteorological Office, Bracknell, U.K.

Published by

European Centre for Medium-range Weather Forecasts
Shinfield Park, Reading, RG2 9AX, U.K.

May 1997